Geological Society, London, Special Publications

3D fracture network dynamics in reservoirs, faults and salt tectonic systems

K. Tuncay, A. Park, D. Payne and P. Ortoleva

Geological Society, London, Special Publications 2003, v.209; p155-175.
doi: 10.1144/GSL.SP.2003.209.01.14

Notes

3D fracture network dynamics in reservoirs, faults and salt tectonic systems

K. TUNCAY, A. PARK, D. PAYNE & P. ORTOLEVA

Laboratory for Computational Geodynamics, Chemistry Building, 800 E. Kirkwood Avenue., Indiana University, Bloomington, IN 47405, USA

Abstract: A unique 3D computer simulator is used to predict natural fracture network characteristics in the subsurface. The model is based on the numerical solution of rock deformation processes coupled to the myriad of other basin reaction, transport and mechanical (RTM) processes. The model integrates seismic, well log and surface geological data to arrive at a quantitative picture of the distribution of fractures, stress, petroleum and porosity, grain size and other textural information.

An important component of the model is an incremental stress rheology that accounts for poroelasticity, non-linear viscosity with yield/faulting, pressure solution and fracturing. It couples mechanics to multi-phase flow and diagenesis (through their influence on effective stress and rock rheological properties, respectively). The model is fully 3D in terms of the full range of fracture orientations and the tensorial nature of stress, deformation and permeability. All rock properties (rheologic, multi-phase fluid transport, grain shape, etc.) are coevolved with the other variables. Examples illustrate the relative importance of various overpressuring mechanisms, lithology and flexure on the location and characteristics of a fracture network.

Fracturing in the subsurface is key to the understanding of many fundamental and applied issues in the geosciences. The objective of this study is to show that these rock failure processes are very dynamic and that this dynamic can only be understood via a model that includes a wide range of other crustal processes. Indeed, the evolution of a fracture network is the result of the interplay of internal processes (matrix texture and pore fluid reactions and flow) and overall tectonic factors. We present results of a unique three-dimensional (3D) model of the coevolution of these dynamic phenomena for use in fundamental crustal studies and the petroleum exploration and production analysis. Fractures and faults affect and are affected by many processes. For example, fractures are affected by fluid pressure and, through their influence on permeability, fractures affect fluid flow and hence fluid pressure. As this is just one of many such 'feedback' relations embedded in the network of geological reaction, transport and mechanical (RTM) processes, a predictive fracture model must be fully coupled (see Fig. 1). As lithologic bodies, folds, domes, salt diapirs and other features are fundamentally 3D, a predictive model of fracture and fault phenomena must be 3D.

Here we present a unique 3D RTM model capable of predicting a host of fracture and fault phenomena. Our model is based on the finite element solution of equations of rock deformation, fracture network statistical dynamics, rock failure and gouge, multi-phase flow, organic and inorganic diagenesis, pressure solution and other compaction mechanisms, and heat transfer. The RTM equations are solved consistent with the influences at the boundary of the basin (sedimentation/erosion, basement heat flux, climate, sea level, and extension/compression or uplift/subsidence history) as suggested in Figure 2.

Key to the attainment of predictive power is the coevolution of all variables. Thus, flow changes fluid pressure which can cause fractures and

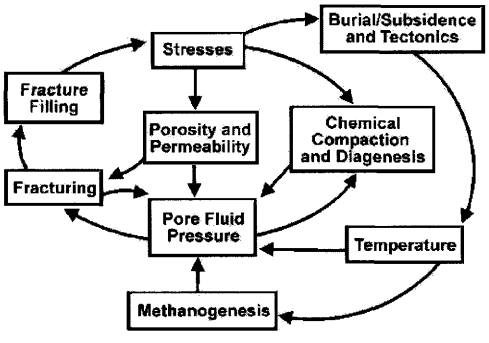

Fig. 1. Complex network of coupled processes underlying the dynamics of a sedimentary basin. These factors and their coupling are accounted for in our unique basin simulator.

From: AMEEN, M. (ed.) *Fracture and In-Situ Stress Characterization of Hydrocarbon Reservoirs*. Geological Society, London, Special Publications, **209**, 155–175. 0305–8719/03/$15.00

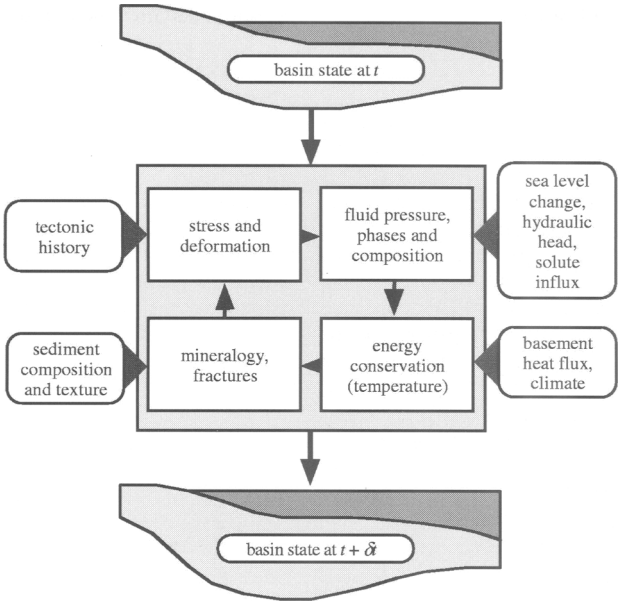

Fig. 2. Schematic Basin RTM flow chart showing the interplay of geological data and the internal RTM processes in evolving a basin over one computational time step.

thereby direct fluid flow along preferred fracture directions. Such coupling and coevolution must be accounted for in their full 3D manifestation. We compute the dynamics of the evolving probability distribution of fracture length, aperture and orientation. Properties such as the permeability tensor are functionals of this probability distribution and constitute a key element of many crustal fluid migration phenomena.

The challenge of modelling fractures and faults in reservoir- or basin-scale systems is one of scale. Typically fractures are metre scale in length and submillimetre scale in aperture. Clearly, it is not feasible to model fractures by introducing a submillimetre scale numerical grid across the reservoir or basin.

The solution is to introduce variables such as average local fracture length, aperture and orientation, characterizing the 'typical' fracture in a macrovolume element of the system. By definition, a macrovolume element is smaller than the scale of the phenomenon of interest (a reservoir) but large enough to contain a statistically significant number of fractures. Such a theory is thus, by nature, a statistical model with the macrovolume element as the sampling volume.

Within such a framework, the variables characterizing the fracture network obey ordinary differential equations in a rock-fixed reference frame (i.e. one moving with the velocity of deformation of the solids). Letting be a collection of texture variables characterizing the fractures as well as the size, shape, orientation, packing, and mineralogy of the grains, we have

$$\frac{D\Theta}{Dt} = \mathrm{A}\left(\Theta, \underline{\underline{\sigma}}, f, T\right) \tag{1}$$

where $\underline{\underline{\sigma}}$ is the stress tensor and f and T are the fluid properties (phase and composition) and temperature in the macrovolume element. In this way fractures (and in general texture dynamics) couple to stress and other factors. Furthermore, rock rheology depends on Θ (as well as f and T), completing a stress/deformation $\Leftrightarrow$ texture feedback. This is just one of the feedback loops contained in Figure 1. Introducing the concept of texture dynamics and capturing the many coupling relations driving the dynamic crustal system is at the heart of our fracture and fault prediction approach. In the remainder of this paper, we illustrate the comprehensiveness and power of our approach using a number of examples. Applications to petroleum exploration and production and the fundamentally 3D nature of many crustal RTM phenomena are noted.

The Basin RTM simulator

Purpose

An overview of our Basin RTM simulator used for fracture and fault modelling is as follows. A complex network of geochemical reactions, fluid and energy transport and rock mechanical (RTM) processes underlies the genesis, dynamics and present-day characteristics of petroleum reservoirs or other crustal phenomena in Basin RTM (see Fig. 1). Basin RTM integrates all the relevant geological factors and RTM processes believed to operate in a sedimentary basin. As reservoirs are fundamentally 3D in nature, Basin RTM is fully 3D.

The RTM processes and geological factors accounted for in Basin RTM are outlined in Figure 2. External influences such as sediment input, sea level, thermal and tectonic effects are allowed to influence the progress of internal RTM processes. Within the basin, these RTM processes modify the sediment chemically and mechanically to arrive at petroleum and mineral reserves, basin compartments and other internal features.

Basin RTM provides a platform for integrating all available geological data as suggested in Figure 2 using the framework provided by the laws of physics and chemistry to facilitate exploration or field development. Available information can be divided into geological data and the physico-chemical rate laws and parameters. The former make a simulation tailored to the specific basin. The physico-chemical information gives Basin RTM the power to predict resource location and characteristics and other features of the evolving basin.

Basin RTM can also be used to carry out sensitivity analyses or to identify new phenomena such as self-organization and other non-linear effects that can dramatically affect the disposition of reservoirs (Ortoleva 1990, 1994*a*). Basin RTM simulations show that the sedimentary basin or other crustal system is highly dynamic, exhibiting a strong degree of autonomy, rather than simply responding to the details of the external influences. As Basin RTM uses data on present-day localtime and characteristics of lithologies to extrapolate these properties beyond the locations of these data, it enhances the use and interpretation of seismic, well log, surface geological and other data to understand the present-day and historical state of the crust. Basin RTM can be used to identify windows of time during which formations along a proposed migration pathway were open, and not blocked due to compaction, fracture closure or diagenetic cementation. Alternatively, Basin RTM can predict if and when a seal was breached and some of the hydrocarbons have escaped due to natural fracturing or permeability-enhancing diagenetic reactions (see Figs 3–5).

How basin RTM works

Basin RTM makes its predictions in a completely self-consistent way through a set of multiphase, organic and inorganic, reaction-transport modules. Calculations of all effects are done self-consistently to preserve all cross-couplings

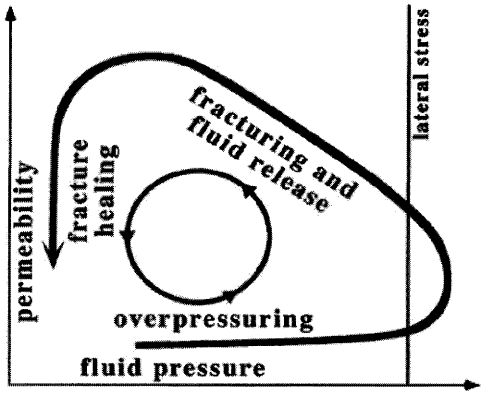

Fig. 3. Fluid pressuring, fracturing and fracture healing feedback cycle, one example of the many feedback mechanisms inherent in the RTM process network. This cycle can repeat many times during a basin's evolution when conditions are appropriate.

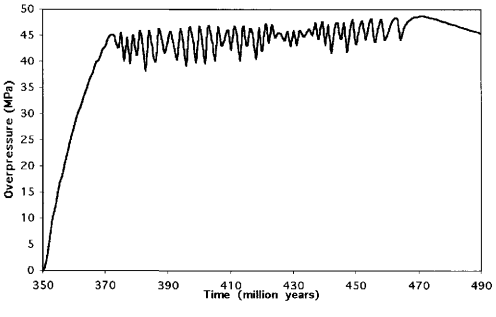

Fig. 4. Overpressure evolution at the bottom of the Ellenburger Formation in Permian Basin, West Texas. Overpressuring starts around 350 million years into the simulation, when fractures in the layer above the source rock disappear. Oscillatory behaviour is a result of cyclic fracturing of the seal driven by petroleum generation. After 470 Ma the cyclic petroleum expulsion ceases and the pressure, oil saturation fracturing and other variables show a more steady behaviour.

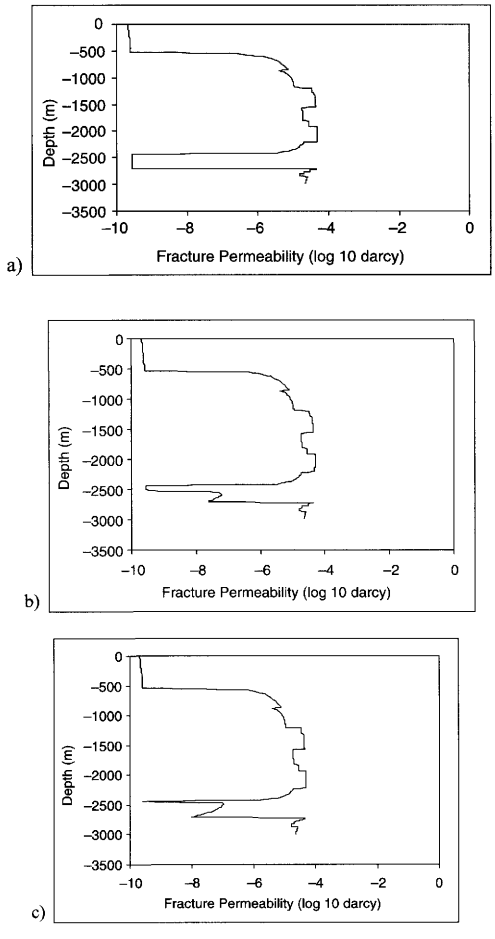

Fig. 5. Fracture permeability profile sequence illustrating the fracture front moving through the seal (between 2450 and 2700 m) Permian Basin, West Texas. Overpressuring of oil and water phases primarily due to oil generation creates a fracture front moving upward through the seal. Once the overpressure is released, the fractures close, which in turn results in descent of the fracture front and overpressuring restarts. This cycle continues until the oil generation rate slows down, or the seal remains fractured due to tectonic effects.

between processes (see Fig. 1). For example, the determination of temperature is affected by transport, which is affected by the changes of porosity that evolve due to temperature-dependent reaction rates. Similarly, the rate of kerogen decomposition depends on temperature which, in turn, depends on thermal transport that is affected, through fluid buoyancy, thermal conductivity, capillarity and relative permeability, by the content of organic material and its thermal decay. All such coupling relations between the full set of RTM processes as in Figure 1 are accounted for in our model.

Predictive power is limited for less rigorous approaches that use statistical correlations. For example, in such methods, porosity history is often based on a formula relating it to mineralogy and depth of burial. However, porosity evolves due to the detailed stress, fluid composition and pressure, and thermal histories. These histories are different for every basin. Thus a simple correlation of porosity with depth and lithologic type does not exist in principle. Basin RTM avoids such problems by solving the fully coupled rock deformation, fluid and mineral reaction, fluid transport and heat transfer problems. Finally, statistical correlations give the average behaviour. As 'on the average' there are no interesting features such as producible pools of petroleum, such approaches can only have a limited interest.

The interplay of geological and physico-chemical information in Basin RTM is suggested in Figure 2. Consider one forward time step in a Basin RTM simulation. The purpose of the incremental evolution step is to advance the state of the basin from a time t to a later time $t+dt$. Two distinct operations take place simultaneously during this time interval dt. The geological information is used to (1) fix the input/output of energy and mass at the basin boundaries and (2) impose the tectonic history (i.e. the overall basin deformation or stress) at the basin boundaries. On the other hand, the physico-chemical processes are used to determine the evolution in dt of the spatial distribution of the local state. The latter describes stress, fluid properties, mineral content, rock texture, permeability, fracture characteristics and temperature.

Basin RTM geological input data are divided into four categories as shown in Figure 2. The tectonic data give the change in the lateral extent and the shape of the basement–sediment interface during δt. As suggested in Figure 2, these data provide the conditions at the basin boundaries needed to calculate the change in the spatial distribution of stress and rock deformation within the basin. This latter physico-chemical calculation is carried out by a stress module that solves equations for incremental stress rock rheology and force balance (see page 167).

The next type of Basin RTM geological data are those affecting the fluid transport, pressure and composition. These fluid data include sea level changes, basin recharge conditions and the composition of fluids injected from the ocean, meteoric and basement sources. This history of boundary input data is then used by the hydrologic and chemical modules to calculate the

evolution of the spatial distribution of fluid pressure, fluid composition and fluid phases within the basin. These physico-chemical calculations are based on single or multi-phase flow in a porous medium and on fluid phase molecular species conservation of mass (i.e., the reaction-transport equations). The physico-chemical equations draw on internal data banks for permeability–rock texture relations, relative permeability formulae, chemical reaction rate laws and reaction and phase-equilibrium thermodynamics.

The spatial distribution of heat flux imposed at the bottom of the basin is another geological input/control. These data as well as the temperature imposed at the top of the sediment pile (i.e. climate and ocean-bottom temperature) are used to evolve the spatial distribution of temperature within the basin during the time interval δt. This evolution is computed using the equations of energy conservation and data for mineral and rock thermal properties (conductivities and specific heats).

The sedimentation data provide the detailed textural characteristics such as grain size, shape, mineralogy, mode and organic texture of the sediment being deposited during dt. This history is automatically computed by Basin RTM using interpreted well log, seismic core and surface data. The physico-chemical laws and data are used to calculate the change of the spatial distribution of mineral and organic texture within the basin during dt. These physico-chemical calculations involve the rate laws for free face grain chemical kinetics, pressure solution and grain rotation or breakage, grain nucleation and the laws of kerogen chemical kinetic transformation. Also used are the laws of fracture nucleation, extension, aperture dynamics and the kinetics of cement infilling.

All these geological input data and physico-chemical calculations are integrated in Basin RTM over many time steps to arrive at a prediction of the evolution history and the present-day internal state of a basin or field. In this way, the physico-chemical laws are used to translate the geological input data into a prediction of the changes of internal basin state and its evolution over a basin's history from its inception (or other chosen initial state) to the present.

Numerical approach

We use the updated Lagrangian approach to solve the time-dependent large deformation problem for geological materials satisfying the incremental stress rheology (Tuncay *et al.* 2000a). In our numerical approach, all variables are referred to the updated configuration in each time step. The approach has two major steps. First, the incremental stress rheology equations are solved at the integration points of the finite elements. Second, the displacements are computed by using a global deformation solver. At each time step, iterations of these two steps are performed until the norm of the change in displacements between two consecutive iterations is less than a specified tolerance. The two-step solution technique allows the introduction of new deformation processes with only minor changes in the code. We use the conjugate gradient iterative technique with a simple diagonal preconditioner to solve for the incremental displacements. The finite element code and iterative solver are parallelized. The details of the finite element formulation are provided in Tuncay *et al.* (2000*a*).

In the multi-phase module, the Galerkin-type finite element approximation is used for saturations, concentrations, and pressures. The non-linear terms and boundary conditions are treated in a fully implicit manner. An upwinding method is developed and implemented in the multi-phase module to stabilize the saturation fronts. The mass matrices are lumped to increase the stability as suggested in previous studies (Huyakorn *et al.* 1994; Abriola & Rathfelder 1993). The computer model accommodates a wide variety of boundary conditions. Because of the highly non-linear behaviour of the equations, a Newton–Raphson technique is employed to solve the non-linear algebraic equations arising from the discretization.

The finite element grid accretes as sediment is added. A new grid layer is added when sediment input causes the top grid layer to become too thick. In contrast, when erosion creates a top layer that is locally too thin, the finite element grid is locally reorganized to preserve numerical accuracy. This accreting, reorganizing grid that also adapts to sedimentary features as they are added or subtracted is required to capture sedimentary detail and ensure numerical stability and accuracy.

The interaction of the top of the sediment pile with the overlying fluids (atmosphere or sea bottom) is accounted for by the value of normal stress and the (assumed) absence of tangential shear. A no-shear lateral boundary condition allows for natural compaction at the sides of the basin. Lateral compression/extension and subsidence/upheaval are imposed at the sides and bottom. The sides and bottom are assumed to be impermeable to fluid flow.

All computational modules are packaged in an overall structure that ensures each equation is

satisfied at every time step. The time step is allowed to change to ensure accuracy and computational efficiency.

Applications of Basin RTM to sedimentary basins

Other basin models have been used to gain valuable insights into the petroleum system. Typically these models are 2D and treat only two or three processes (Ungerer *et al.* 1990; Larson *et al.* 1993; Maubeuge & Lerche 1993, 1994; Roberts & Nunn 1995; Schneider *et al.* 1996; Luo & Vasseur 1996; Luo *et al.* 1998; Wang & Xie 1998). Consequently, they are not sufficiently comprehensive to accurately simulate natural sedimentary systems and, in particular, fracture networks.

Fracture-mediated petroleum expulsion, migration, and escape from reservoirs are key aspects of the dynamic petroleum system (Figs 3–5). In most of the existing basin evolution models, it is assumed that rocks fracture when the fluid pressure exceeds a specified fraction of lithostatic stress (Maubeuge & Lerche 1993, 1994; Roberts & Nunn 1995; Wang & Xie 1998). This assumption ignores the dependence of fracturing on lithologic properties. In our studies, we find that fracturing strongly depends on rock composition and texture, including mineralogy, grain size, and porosity which indirectly affect the stress tensor (Figs 6 & 7). Another limiting assumption is that there exists a simple dependence of porosity on effective stress (Ungerer *et al.* 1990; Maubeuge & Lerche 1993, 1994; Roberts & Nunn 1995; Luo & Vasseur 1996; Schneider *et al.* 1996; Wang & Xie 1998). This results in a very smooth porosity profile but ignores the dependence of porosity on rock composition and texture. In our approach, porosity is obtained by both solving the mass balance equation for solids and computing rock deformation velocity using a multi-process, incremental stress rheology that contains the elastic and viscous parameters which are functions of texture and composition. By coupling mass balance algorithms with our porosity and stress solvers, porosity and stress are computed self-consistently. As a result, shales usually have lower porosity, and higher least compressive stress than sandstones (Fig. 7). The small grain size combined with low porosity results in very low permeability and thus these layers can form efficient seals. Furthermore, our results show that low shear viscosity/bulk viscosity ratio makes fracturing very unlikely in the absence of flexure or extreme overpressuring mechanisms, such as petroleum generation or fluid thermal expansion.

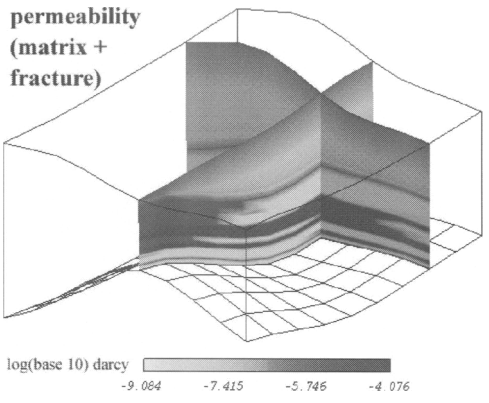

Fig. 6. Predicted cross-sections of permeability at 45 Ma from a simulation of Piceance Basin, Colorado. The system is 50×48 km wide and 1 to 3 km deep. Different permeabilities reflect varying sediment compositions including porosity, texture and mineral grain sizes, plus that resulting from fractures. The computation was carried out on an accreating, lithology-adapted hexahedral grid which at the final time was 20x20x60 elements. The uplift/subsidence, erosion and sedimentation histories were computed using tops, core, and well log data provided by DOE and Barrett Resources. Lateral compression/extension effects were not accounted for in the simulation.

In other basin evolution simulators, fracture permeability is assumed to be isotropic. This simplification ignores the fact that, for an accurate description of fracture orientations, the full stress tensor as well as irreversible (e.g., viscous-like rather than purely elastic) behaviour must be known (Fig. 8). Also disregarded is the interaction between the deformation/stress computation and fracturing. Rocks fracture due to the difference between fluid pressure and least compressive stress. But as fractures open, overall rock volume increases and fluid pressure in the fractures compresses the rock, increasing the compressive stress normal to the fracture plane. Thus, fracturing is a self-limiting process: firstly, as fractures open, they provide a pathway for fluid escape; and secondly, the volumetric strain caused by fractures increases the confining stress that reduces the rate of fracture growth (Tuncay *et al.* 2000*a*,*b*).

Although one- and two-dimensional studies give hints about the dynamics of basin evolution, a three-dimensional basin simulator is necessary to take three-dimensional geometric effects into account (Figs 6 & 9). This becomes extremely important when fracturing is due mainly to flexure and the direction of tectonic compression/extension is changing during the basin's history. Fracture networks provide a pathway for

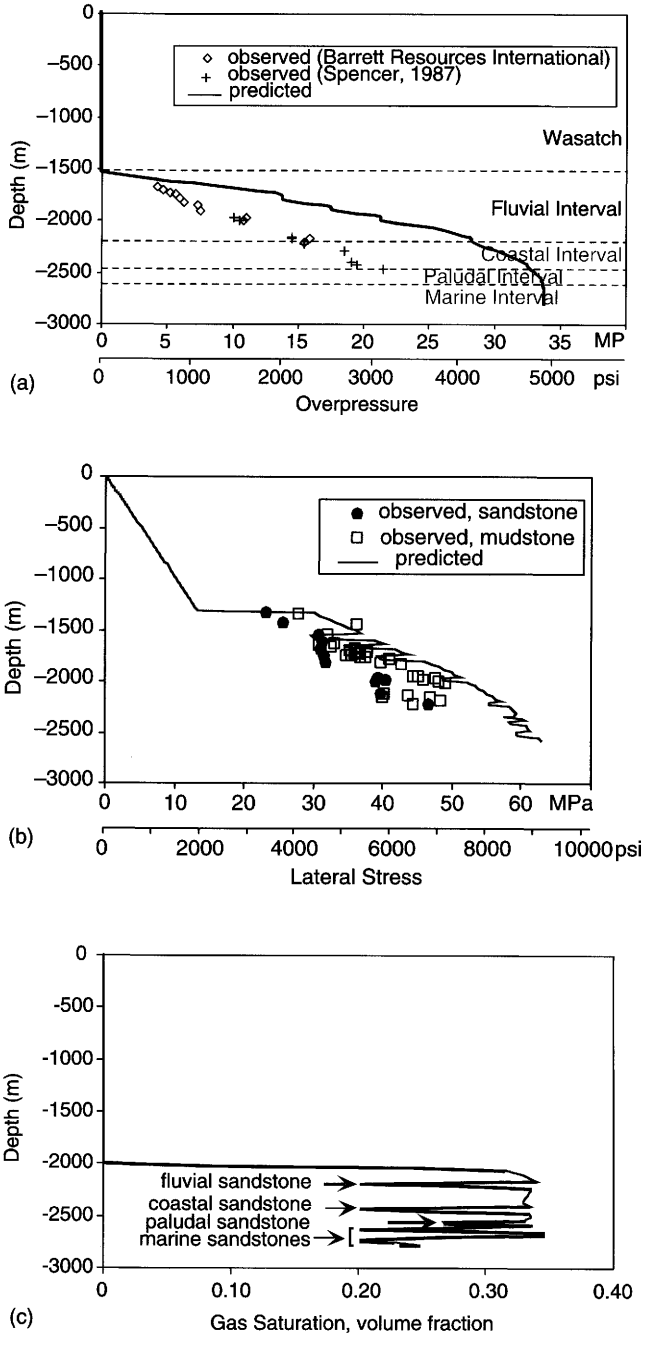

Fig. 7. Simulations by Basin RTM show good agreement with observations. Shown are present-day fluid pressure (**a**) and least compressive stress (**b**) at the MWX site, Piceance Basin, Colorado, compared with observations. In sandstones, the lateral stress and fluid pressures are found to be similar, indicating their vulnerability to fracturing whereas in the mudstones lateral stress exceeds fluid pressure, underscoring the lack of fracturing in them at present day (as observed). Our predictions also show that this situation is dynamic: during an epoch in the past, some of the mudstones were also fractured in some areas in the Piceance Basin as suggested in the literature. (**c**) Predicted natural gas saturation (from Payne *et al.* 2000).

fluid flow and, especially in layered rocks, fluids can move laterally out of the vertical plane. Appropriate simulations can be accomplished only by a three-dimensional basin simulator with a stress/deformation solver that can capture non-planar effects and strong contrasts in rheology from layer to layer.

Although the history of temperature, sedimentation rate, and subsidence rate are among the most important parameters that affect the evolution of a basin, some basin simulators start with a pre-defined grid (Schneider *et al.* 1996). In other words, two basins with the same final thickness and lithology but different time history are assumed to behave similarly. This approach ignores the time-dependence of, for example, overpressuring which often correlates with sedimentation rate and is a key factor in fracturing as well as deformation (Wang & Xie 1998; Ortoleva 1998).

Another limitation of previous models is the absence of shear failure. Only a few models consider the contribution of mechanical shear to rock failure (Luo *et al.* 1998; Larson *et al.* 1993). However, these models are limited to two dimensions. In our model, a Drucker-Prager-type failure function is used to build in a shear failure via a transition in rock viscosity. The coefficients of the failure function have been fitted with experimental data (Sakrani 1996; Ozkan *et al.* 1998). The shear viscosity is assumed to depend on the failure function and texture. As the rock approaches failure, shear viscosity decreases. This feature extends the applicability of our basin simulator to fault formation problems (Fig. 10). We have already made an attempt to include the rate of strain due to gouge (Fig. 11) to show the effect of shearing on the particle size distribution and porosity (Ozkan *et al.* 1998; Ozkan & Ortoleva 2000).

Our model accounts for the changing rock rheological parameters that accompany the changing lithologic and fracture properties. The bulk, shear and effective stress coefficients of the (assumed) isotropic rocks are computed using Berryman's composite medium theory (Berryman 1980, 1986). In our approach, by assuming that the shear and bulk viscosities depend on grain contact areas, rheology is computed as a function of the mechanically and diagenetically modified texture. Thus, dynamic rheologic properties are used to compute basin stress/deformation history using an incremental stress rheology (Zienkiewicz & Cormeau 1974; Rice 1975) extended by the authors(Tuncay *et al.* 2000a,b; Ortoleva 1994*a*, 1998).

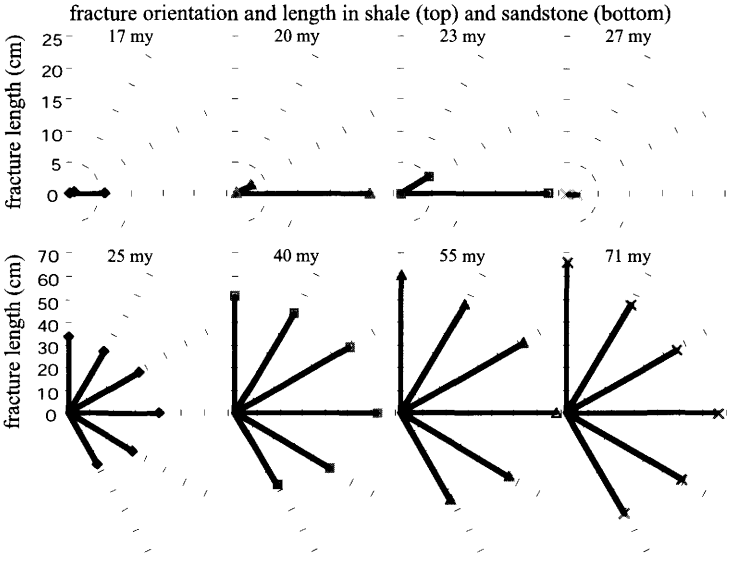

Fig. 8. Predicted fracture orientations and length in a shale (top) and a sandstone (bottom) from the Piceance Basin simulation of Fig 6. Changing sediment properties, stress and fluid pressure during the evolution of the basin result in dynamic fracture patterns, which in turn significantly affect the anisotropy of fracture permeability. If the enhanced permeability from fracturing is significant, it can direct the flow of petroleum; understanding such occurrences of the past, therefore, can be important for identifying or understanding reservoirs in presently unlikely structural and stratigraphic locations.

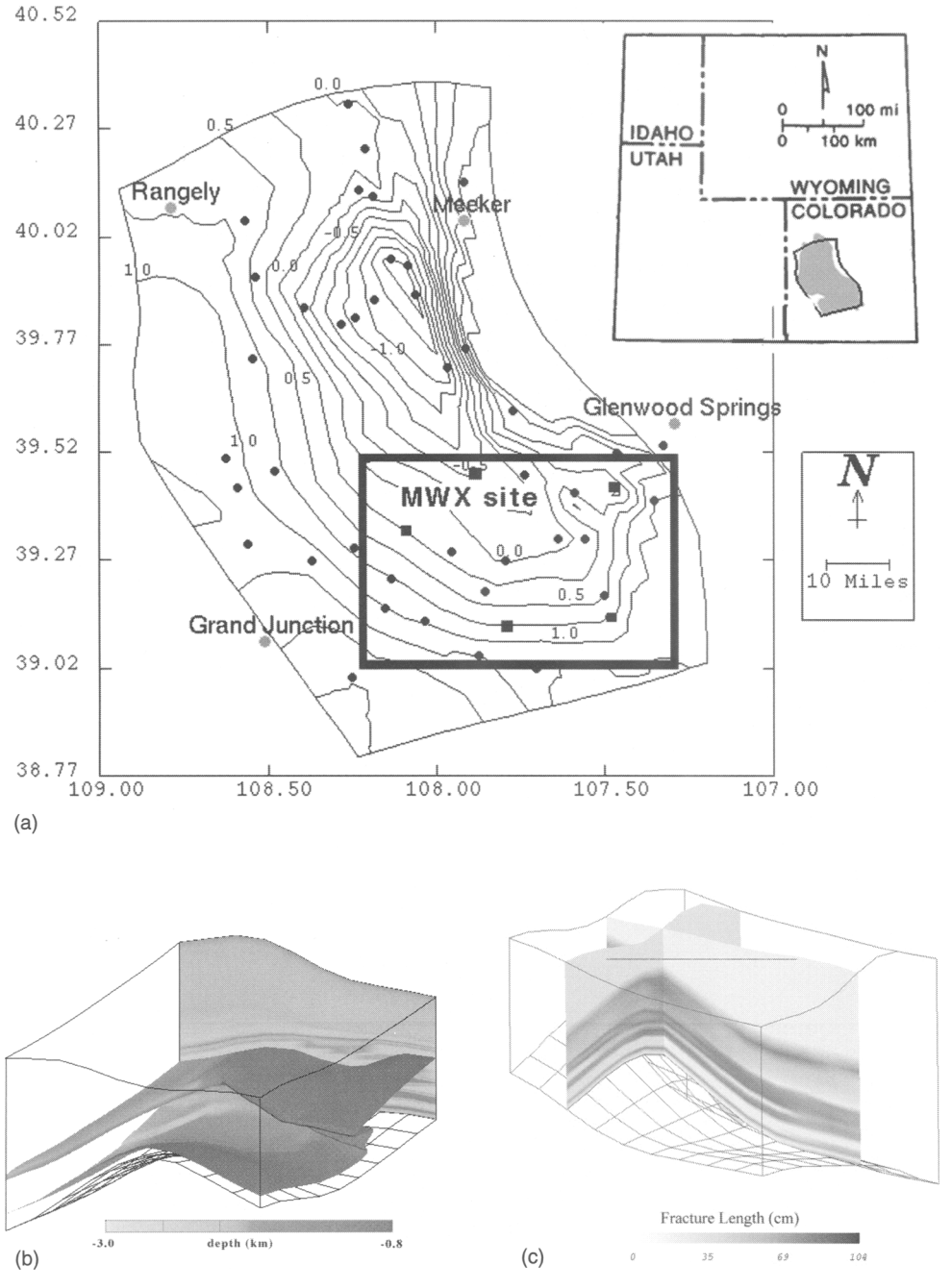

Fig. 9. (**a**) Simulation domains for basin-scale and inter-field studies (thickly outlined box) of Piceance Basin simulations. The Rulison Field is in the upper northwestern area of the latter box. (**b**) Isosurface of overpressure (15 bars) shaded with depth. The folded, multi-layered structure is dictated by the interplay of lithological differences and fracturing and shows the three-dimensional complexity of conductivity of overpressured zones. Thus, stacked overpressured compartments as viewed as a simple pressure–depth curve may hold little insight into the full three-dimensionality of the structure. (**c**) The distribution of fracture length reflects lithologic variation and the topography imposed by the basement tectonics. The layered fracture length structure is closely related to the layering in overpressure surface (from Tuncay *et al.* 2000*a*).

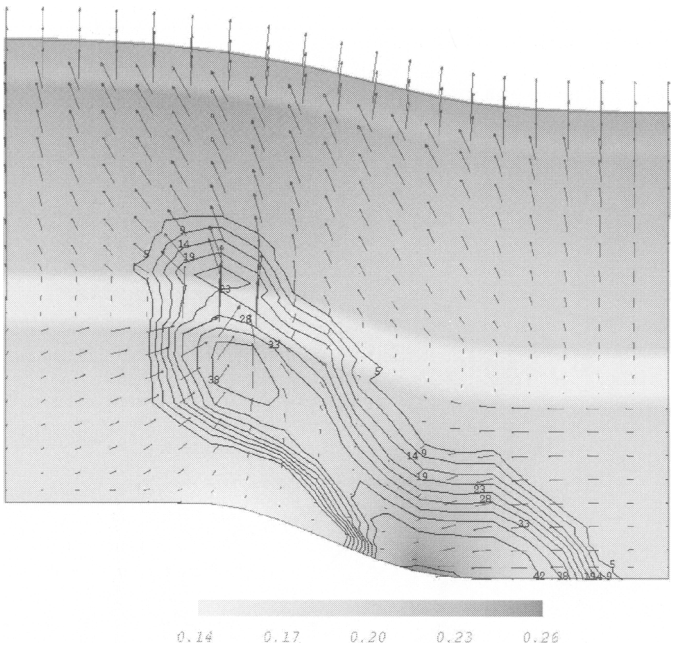

Fig. 10. Cross-section of a 2D, 5×2.5 km normal fault system after 5 My of simulation. The shading indicates porosity and shows differences between the four lithologies; the shales (low porosity) are at the middle and top of the domain. Higher porosity regions (in the lower-right and upper-left corners) and the fracture length (contour lines) arose due to the deformation created by differential subsidence. Both stress field and fracturing are strongly affected by rock composition and texture. The arrows indicate fluid flow toward the region of increasing porosity (lower-right) and through the most extensively fractured shale.

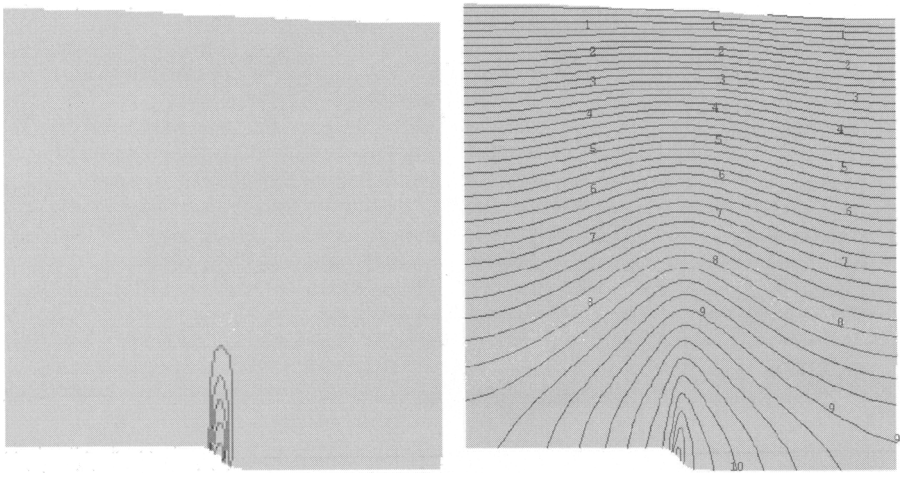

Fig. 11. The effect of gouge on **(a)** porosity and **(b)** overpressure. The size of the domain is 3 km by 3 km in cross-section. The fault width is 0.1 km and the rate of faulting is 0.2 km My^{-1}. To isolate the effect of gouge on the pressure and texture, a very high bulk viscosity is used. Therefore, the only overpressuring mechanism present is the gouge-related changes in the texture. The weakness of the San Andreas Fault is attributed to high fluid pressures in the fault zone (Byerlee 1990; Rice 1992). This example demonstrates fluid flow and deformation interactions in basin environments.

Salt tectonics

Salt movement in the subsurface can dramatically affect the distribution and character of fracture zones and faults for several reasons:

- salt diapirism and related phenomena can cause flexure and otherwise dramatically affect the stress regime in the neighbouring sediments;
- salt movement can affect the topography of the sea floor and thereby the geometry and lithologic character of the salt-adjusted sediments;
- salt is of vanishingly small permeability and therefore can isolate high overpressure (up to lithostatic) and thereby influence effective stress in the underlying sediments; and
- by distorting the heat flux, changing the salinity, and altering the fluid flow patterns, salt can change the diagenetic history and, thereby, rock mechanical properties.

As salt withdrawal is believed to be an important factor in fracturing in some areas, we have incorporated advanced salt tectonics modelling into Basin RTM by calibrating our rheology to be consistent with salt deformation experiments.

With this, our simulator can address the following exploration and production challenges:

- predict the location and geometry of faults or zones of fracturing created by salt motion;
- predict the morphology of sedimentary bodies created by salt deformation;
- locate pools of petroleum or migration pathways created by salt tectonics; and
- assist in the interpretation of seismic data in salt tectonic regimes.

The interplay of salt deformation with the rheology of the surrounding strata is key to understanding the salt deformation and reservoir location and characteristics relationship. The continuous and discontinuous (i.e. fauting and fracturing) responses of the surrounding sediments are induced by salt movement. In turn, the deformation of these sediments promotes or inhibits salt motion.

Figure 12 shows a cross-section of a Basin RTM-simulated salt wave. Note the relationship among deformation, fluid flow and fracturing. The orientation of fracturing follows salt morphology. Fluid flow patterns are strongly influenced by salt morphology and associated fracture patterns. In this case and those to follow, the salt deformation is due to the interplay of salt buoyancy, salt modification of the distribution of the rate of sedimentation and the overall tectonics (i.e. basin extension/compression and upheaval/subsidence).

To predict salt tectonics-related petroleum pools, one must co-evolve petroleum generation/

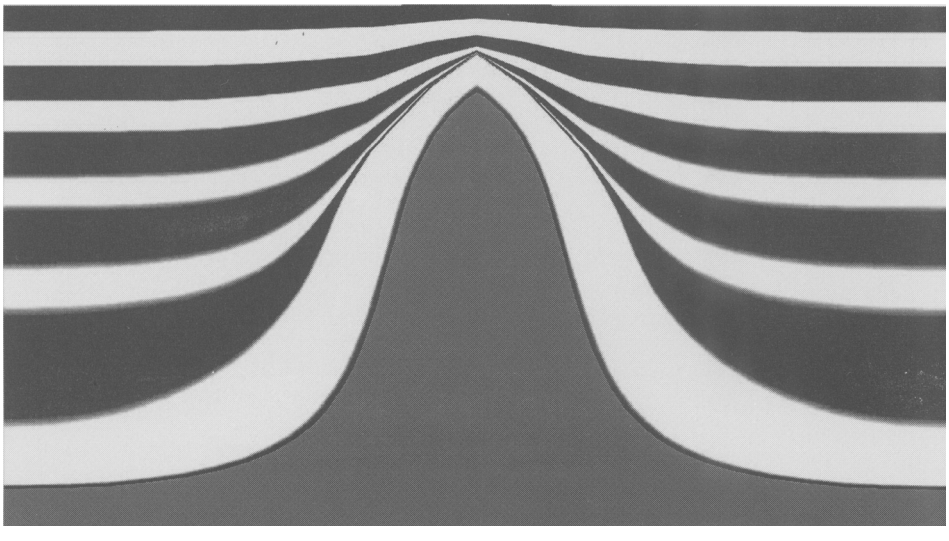

Fig. 12. Basin RTM simulated salt wave showing associated deformation (as indicated by the shape of the evolved salt body). Shown is the state after 8 My of deformation and sedimentation. The salt bed originally only had a 400 m topographic contrast. There are alternating layers of sandstones and shales above the salt at this stage. The salt tectonic – sedimentation interaction induced the sediment geometry and the generation of mini-basins at the flanks of the wave.

expulsion/migration with salt and rock deformation. Figure 13 shows an oil pool developed in association with salt diapirism. The oil was generated in a source rock overlying the salt, both of which were essentially flat in an early stage that preceded diapirism. A similar situation but for a subsalt source rock is seen in Figure 13. In both cases, the influence of salt motion on fracturing and porosity strongly affects migration and ultimate reservoir quality. The escape of subsalt oil at the edges of the salt lens is also seen in Figure 14. Salt tectonics is, for the most part, a fundamentally 3D phenomenon. An example of a simulated salt diapir in 3–D view is seen in

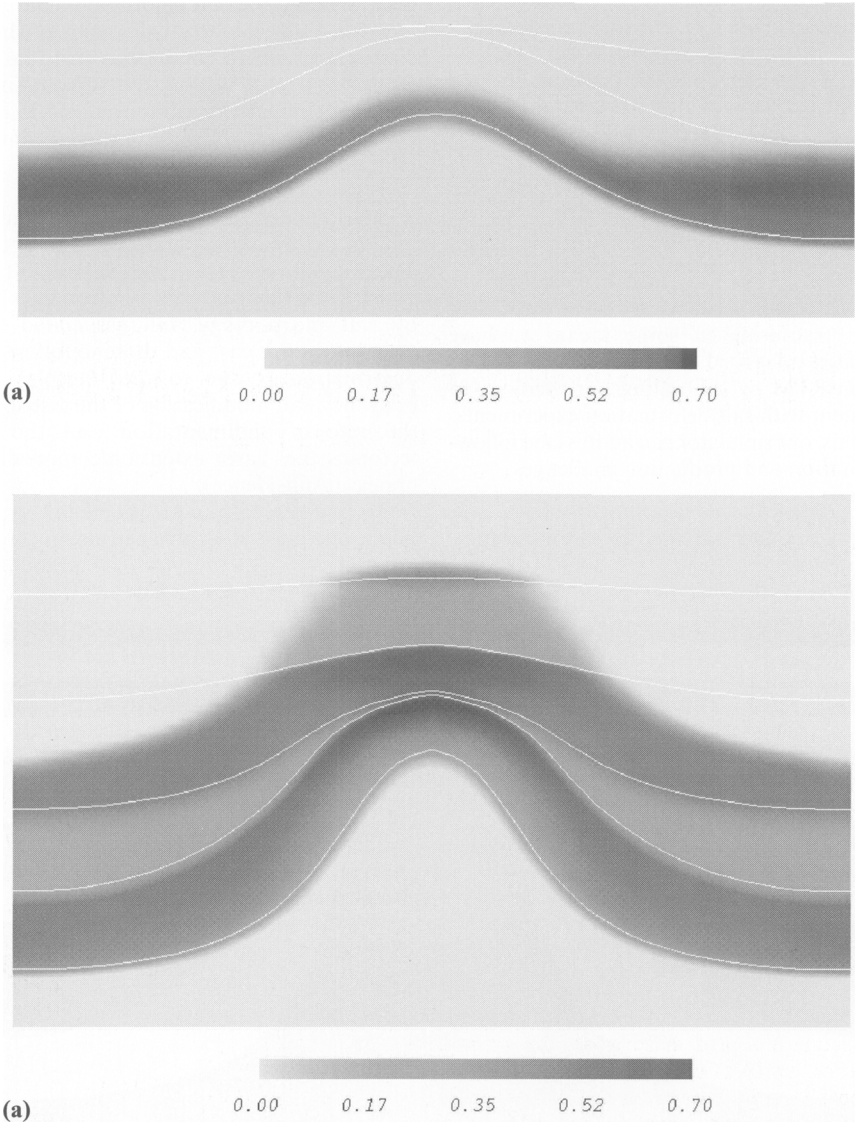

Fig. 13. Simulated time sequence (1.46 (**a**) and (**b**) 3.76 My into the simulation) of oil saturation overlying a rising salt dome. Source rock overlying the dome was transiently overpressured and fractured, facilitating upward oil migration within it and into the overlying layers. Orientations of long-lived fractures (residing in the sandstones) illustrate the relationship between the salt motion and fracture pattern. The location of oil strongly depends on the rate of salt motion and the coevolving mechanical and transport properties of the adjacent sediments.

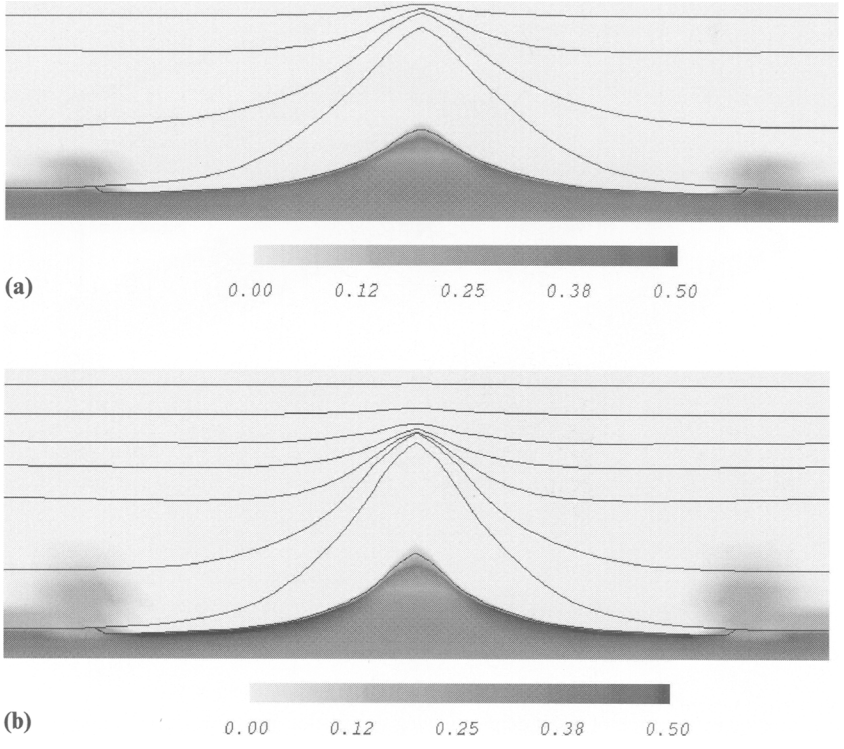

Fig. 14. As in Figure 13 except for an initially finite size (lenticular) salt body and in addition the co-evolution of subsalt petroleum (3.12 (**a**) and 5.56 (**b**) My into the simulation). Shown is the oil saturation with curves indicating lithologic contacts. The overpressure under the salt body and the stress regime on the underlying sediment have preserved porosity in the centre region under the salt while the compaction under the edge of the salt led to the formation of a seal. Thereby a subsalt compartment is formed.

Figure 15. Note the pockets of fracturing associated with the salt diapir. These and other Basin RTM simulations of salt phenomena illustrate the ability of our approach to predict fractures related to salt tectonics. The details of the salt tectonics simulations are provided in Tuncay & Ortoleva (2000).

Incremental Stress Rheology, Statistical Fracture Dynamics and Rock Competency

Incremental stress rheology

The strongly coupled nature of the crustal deformation problem can be captured using an incremental stress rheology. The specific rheology used in our modelling integrates most of the strain mechanisms believed to operate in the crust. It has the form (Tuncay *et al.* 2000*a*,*b*; Ortoleva 1994*a*, 1998; Ortoleva *et al.* 1997)

$$\dot{\underline{\underline{\varepsilon}}} = \dot{\underline{\underline{\varepsilon}}}^{el} + \dot{\underline{\underline{\varepsilon}}}^{vp} + \dot{\underline{\underline{\varepsilon}}}^{ps} + \dot{\underline{\underline{\varepsilon}}}^{fr} + \dot{\underline{\underline{\varepsilon}}}^{go} \tag{1}$$

Here, $\dot{\varepsilon}^{Y}$ is the net rate of strain while the terms on the right-hand side denote the contributions of five processes: poroelasticity (el), continuous viscoplastic (vp), pressure solution (ps), fracturing (fr) and gouge (go). Specific expressions for each term have been taken from the literature. In this study we consider poroelasticity and continuous viscoplasticity.

The poroelasticity rate of strain $\dot{\varepsilon}^{el}$ may be expressed in terms of stress $\underline{\underline{\sigma}}$, pressure p of the (assumed single) fluid phase, and rock texture Θ via:

$$\dot{\underline{\underline{\varepsilon}}}^{el} = \underline{\underline{\underline{\underline{C}}}}^{-1}(\Theta)\frac{D}{Dt}\left(\underline{\underline{\sigma}} + \alpha(\Theta)p\underline{\underline{I}}\right) \tag{2}$$

where $\underline{\underline{\underline{\underline{C}}}}$ is the fourth rank tensor of poroelastic coefficients, α is the effective stress coefficient, and I is the second rank identity matrix. Here, D/Dt represents a material time derivative measuring the rate of change of a tensor in time

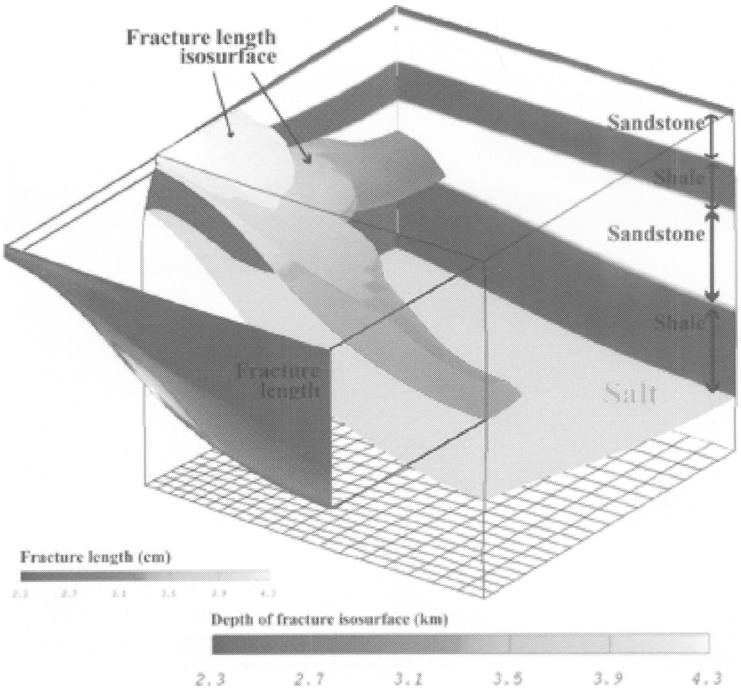

Fig. 15. Simulated quarter section of a salt diapir showing the relationship to fracturing in the overlying sandstones after 3 My of deformation. Extracted partial front cross-section shows the fracture length.

with respect to a local reference frame fixed to a translating, rotating material volume element. The texture Θ represents a set of variables characterizing the mineralogy, shape, size, orientation and packing of the grains of each mineral. The bulk and shear moduli of the drained porous medium, and the effective stress coefficient of the medium can be computed in terms of the Θ and mineral elastic properties using Berryman's (1980, 1986) approach.

The inelastic mechanical contribution to $\dot{\varepsilon}$ is cast in the present approach as a non-linear viscosity law in the form:

$$\underline{\underline{\dot{\varepsilon}}}^{(vp)} = \underline{\underline{\underline{\underline{\eta}}}}^{-1}\left(\underline{\underline{\sigma}} + \tilde{\alpha} p \underline{\underline{I}}\right) \tag{3}$$

The fourth rank viscosity tensor $\underline{\underline{\underline{\underline{\eta}}}}$ depends on stress, fluid pressure and texture. The second term in the effective stress involves a coefficient that is usually taken in the literature to be unity. The shear viscosity is assumed to be a strong function of rock competency. Sleep & Blanpied (1994) assumed that the viscosities depend on the intrinsic viscosity of grains and the volume fractions of pores and fractures. However, they did not consider the sudden drop in the shear viscosity due to failure, which is one of the key parameters required to model the stress drop following rupture. We expect that in the case of failure, the change in the shear viscosity is greater than the change in the bulk viscosity. Since the state of stress is strongly dependent on the viscosity ratio, this feedback might play an important role in the reorganization of fault zones after failure.

The texture must be further augmented when rock competency is considered. This is described in the following section. Again, in the spirit of our Markov approach, only when it is sufficiently comprehensive can a self-consistent deformation model be set forth. One expects that $\dot{\varepsilon}^{(j)}$ (j=poroelasticity, viscosity, pressure solution, fracturing, gouge, etc.) should depend on all the aforementioned variables . With this:

$$\underline{\underline{\dot{\varepsilon}}} = \sum_{j=1}^{N_d} \underline{\underline{\dot{\varepsilon}}}^{(j)}(\Theta, \underline{\underline{\sigma}}, p, c, T) \tag{4}$$

for a system with N_d deformation mechanisms. The dependence of the strain rates on state

clarifies the central role of incremental stress theory in integrating all the crustal RTM processes into a unified model. It is the coupling allowed by this integration that underlies fault dynamics.

The total rate of strain $\dot{\varepsilon}$ is defined as:

$$\dot{\varepsilon}_{ii'} = \frac{1}{2}\left(\frac{\partial u_i}{\partial x_{i'}} + \frac{\partial u_{i'}}{\partial x_i}\right) \tag{5}$$

for rock deformation velocity $\underline{u}$ and Cartesian coordinates *xi*, *xii*, *xiii*. The six independent components of the symmetric second rank tensor (Equation 2) must be supplemented with three additional equations so that the three deformation velocity components ($\underline{u}=u_1,u_2,u_3$) and the six independent stress components can be determined. The required condition arises from force balance:

$$\sum_{i'=1}^{3} \frac{\partial \sigma_{ii'}}{\partial x_{i'}} + f_i = 0 \tag{6}$$

for body force f_i which is given by:

$$f_i = g\rho_m \delta_{i3} \tag{7}$$

Here g is the gravitational acceleration, ρ_m is the crustal mass density, and the subscript $_3$ denotes upward direction.

In addition to the coupling of deformation to other phenomena through the incremental stress rheology, there are numerous indirect couplings. For example, rock properties such as permeability, multi-phase flow parameters, reactive grain surface area and thermal conductivity depend strongly on texture. As the latter is affected by stress and deformation, a complex network of coupling relations is thereby expressed. For further discussion of the consequences of this network, see Ortoleva (1994*a*,*b*, 1998), Tuncay *et al.* (2000*a*,*b*) and Dewers & Ortoleva (1994).

Rock Competency

Predicting faulting and other rock failure phenomena requires a model that accounts for rock competency. We have introduced a measure of rock competency that accounts for the degree to which grains are attached to each other (Tuncay *et al.* 2001). Schematically, the theory is as follows.

Let Γ, rock competency, measure the fraction of grain surface that is attached to other grains. Thus Γ is in the range $0 \le \Gamma \le 1$. Large Γ implies competency while in a low Γ rock there are few intact grain–grain contacts. Thus rheologic quantities such as rock strength or viscosity are strongly dependent on Γ.

Schematically, our model is as follows. The equation of motion of Γ is taken in the form:

$$\frac{D\Gamma}{Dt} = R(\Gamma, F) \tag{8}$$

where F is a failure function that depends on macroscopic stress, fluid pressure, rock texture, mineralogy and temperature. In three dimensions, the failure function is assumed to take the form (Drucker & Prager 1952):

$$F = aJ_1 + \sqrt{J_2} - b \tag{9}$$

where J_1 is the first invariant of the effective stress tensor and J_2 is the second invariant of the deviatoric effective stress tensor. The coefficients a and b can be expressed in terms of angle of internal friction φ and cohesion C determined from conventional triaxial compression experiments (Desai & Siriwardane 1984):

$$a = \frac{2\sin\varphi}{\sqrt{3}(3-\sin\varphi)} \tag{10}$$

$$b = \frac{6C\cos\varphi}{\sqrt{3}(3-\sin\varphi)} \tag{11}$$

Here, we assume that cohesion depends on rock competency. For an intact rock ($\Gamma=1$), b is large. As the rock competency is lost, the cohesion-like term b vanishes. Therefore b is a strong function of Γ taken here to be $b=b^*\Gamma^n$ where b^* refers to the value when $\Gamma=1$ and n is a phenomenological exponent.

If the dynamics of Γ is relatively fast, its evolution is closely related to the shape of the curve $R(\Gamma,F)=0$ (see chapters 2 and 3 of Ortoleva (1992) for further discussion). The Γ dynamics is, in a sense, a cooperative phenomenon, i.e. a decrease in competence fosters more rapid decline. This is captured by the qualitative picture of Figure 16 where a schematic evolution path in the F,Γ plane is shown.

Through this model, failure is rapid while healing can be a much slower process. This follows if R is relatively small when Γ is small and F is less than a healing value F_h. This type of effect gives geological materials the memory they

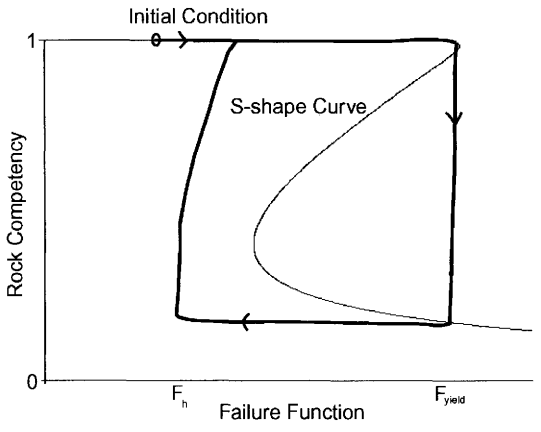

Fig. 16. Schematic competence (Γ) and failure function (F) plane illustrating the cooperative aspects of rock failure. When Γ is near unity, the rock is competent but when F exceeds F_y, it is compromised. However, for $F<F_h$, competence is regained through chemical healing processes.

have of zones of earlier faulting. Here, $R(\Gamma,F)$ is taken in the form

$$R(\Gamma,F)=k(\Gamma,F)\left(\begin{matrix}-F+d_3(\frac{1}{2}-\Gamma)+\\ \frac{d_2}{\Gamma}+\frac{d_1}{1-\Gamma}+d_4\end{matrix}\right)\Gamma(1-\Gamma) \qquad 12$$

where d_1,d_2,d_3 and d_4 are material constants. The function k is chosen such that when Γ is small and $F<F_h$, k is small, ensuring that healing is slow. Finally, F_h can be determined in terms of d_1,d_2,d_3 and d_4. Conceptually, these parameters depend on mineralogy, grain size, shape and packing.

We now show that the feedback associated with the coupling of shear stress (via incremental stress rheology) and rock competency naturally supports autonomous oscillation. Consider a simple shear system with the total rate of strain given by the sum of poroelastic and non-linear viscous contributions. The rate of strain due to poroelasticity can be written in terms of the total rate of strain and rate of strain due to viscosity as $\dot{\varepsilon}^{el}=\dot{\varepsilon}-\dot{\varepsilon}^{vp}$. Assuming isotropic simple shear, the following ordinary differential equation for the shear stress is written:

$$\frac{D\tau}{Dt}=\frac{G_f}{\mu(\Gamma)}(2\dot{\varepsilon}\mu(\Gamma)-\tau) \qquad (13)$$

where τ, $\dot{\varepsilon}$, G_f and μ are the shear stress, total rate of shear strain, elastic shear modulus and shear viscosity, respectively. Shear viscosity is taken to be an increasing function of rock competency $\mu=\mu^*\Gamma^m$. The exponent m is taken as 8 to capture the large change in the order of magnitude of shear viscosity between intact and failed rock. For simplicity, assume that the failure function is in the form $F=|\tau|-c$. In this case c is taken to be $c=-a(\sigma_n+p)+b^*\Gamma$ where σ_n and p are the normal stress (positive in tension) and fluid pressure, respectively. The coefficient b^* is taken to be 50 MPa within the range of typical rock properties. Note that for small values of Γ, $F\oplus|\tau|+a(\sigma_n+p)$, capturing the usual friction law. The term $-a(\sigma_n+p)$ is taken as 30 MPa. The rate of shear strain is either taken to be a specified function of time or determined by the energy dissipation condition

$$\tau\dot{\varepsilon}=E \qquad (14)$$

where Ė is the rate of energy input.

Equations (8) and (13) form a strongly coupled set of non-linear ordinary differential equations for the shear stress and rock competency that were integrated numerically by the fourth-order Runga-Kutta technique with adaptive time stepping. Setting the RHS (Equation 13) to zero yields for constant Ė and the Drucker Prager failure function (Equation 9):

$$\Gamma=\left(\frac{(F+c)^2}{2\mu^*\dot{E}}\right)^{1/m} \qquad (15)$$

Fig. 17 illustrates the null curves for different values of $\dot{E}$. For small $\dot{E}$ the stress null curve (Equation 15) intersects the S-shaped null curve $R=0$ on the upper stable branch near $\Gamma=1$ (competent rock), i.e. the competent rock viscosity μ^* is sufficiently low that the rate of energy input is equal to the rate of viscous energy dissipation (ductile flow). For very large $\dot{E}$, rock fails but the null curves intersect at the lower stable branch, i.e. the rock remains failed because of the very low shear viscosity needed to dissipate the required energy (aseismic faults). For intermediate values of $\dot{E}$, the null curves intersect at the unstable branch of $R=0$. In this case, for a constant $\dot{E}$, rock fails and heals cyclicly (seismic faults). It is also possible that the null curves intersect at three distinct points. In this case, depending on the initial conditions of shear stress and rock competency, rock will either never fail or never heal. If a point F,Γ is above the null curve given by Equation 15, the shear stress increases, otherwise it decreases. Similarly, if a point (F,Γ) is to the right of the null curve $R=0$, the rock competency decreases. These four cases suggest a classification of fault dynamics: intact stable sliding, failed stable sliding, multiple state and oscillatory sliding.

The above model can support autonomous oscillatory failure reminiscent of the earthquake cycle when the null curves intersect on the unstable (middle) branch. Figure 18 shows the F,Γ plane for an oscillation-supporting set of parameter values ($\dot{E}=0.06$ GPa Ma^{-1}). The arrows show the direction of movement. Figure 18 illustrates the predicted time dependence of rock competency (Fig. 18a) , failure function (Fig. 18b) and shear stress (Fig. 18c). As seen in Figure 18, after a short transient period, the system finds its limit cycle. The stress drop after failure is quite large because of the use of Equation (14). It is likely that in two- and three-dimensional simulations, the stress drop will be less due to the interaction of failed and unfailed regions. Furthermore, the frequency of failure events is expected to increase since the energy release at each failure (stress drop) will be less.

Fracture Network Statistical dynamics

We have developed a model of the probability for fracture length, aperture and orientation (Tuncay *et al.* 2000*b*). The model predicts the evolution of this probability in response to the changing stress, fluid pressure and rock properties as the basin changes. The fracture probability is used to compute the permeability tensor. The latter affects the direction of petroleum migration, information central to planning infill drilling spacing and likely directions for field extension. It is a key to the design of horizontal wells and the optimum rate of production in stress-sensitive reservoirs. Finally, the predicted dis-

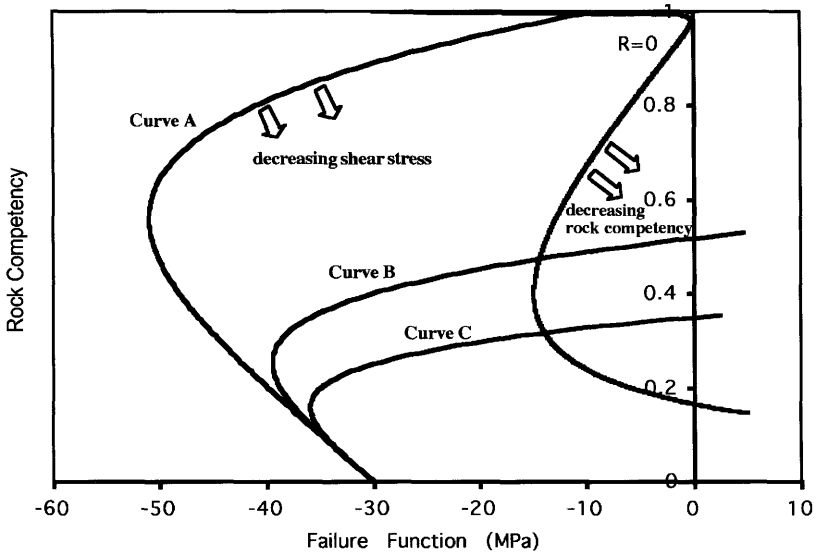

FIG. 17. The null curves and phase diagram for a time-dependent $\dot{E}$ (0–100 years, $\dot{E}=1$ GPa Ma^{-1}; 100–200 years, $\dot{E}=100$ GPa Ma^{-1}; 200–300 years, $\dot{E}=50$ GPa Ma^{-1}; 300–400 years, $\dot{E}=100$ GPa Ma^{-1}; 400–600 years, $\dot{E}=1$ GPa Ma^{-1}).

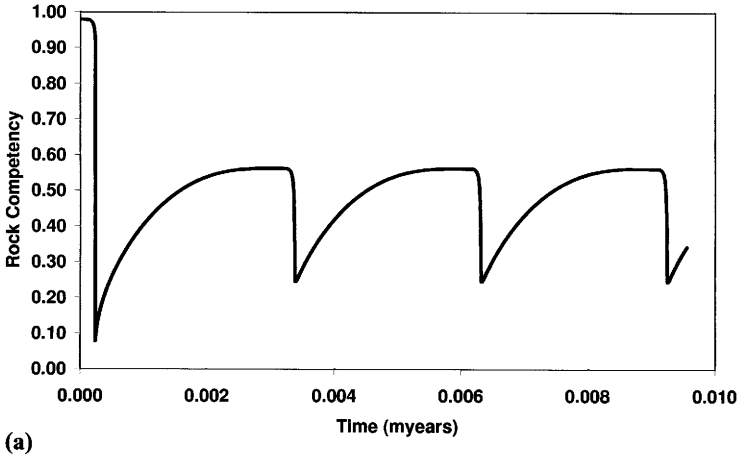

(a)

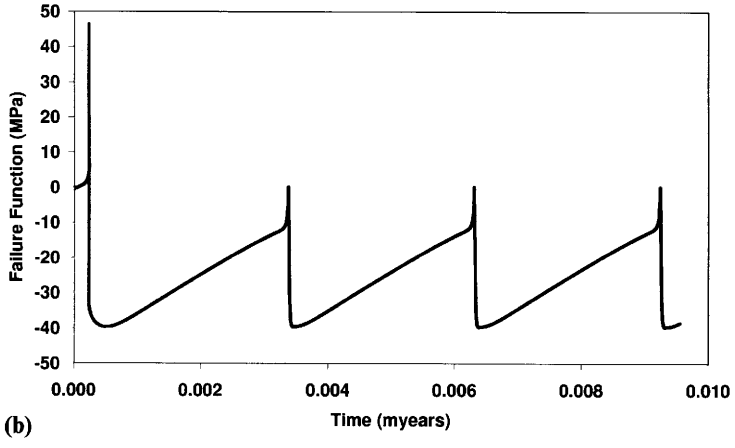

(b)

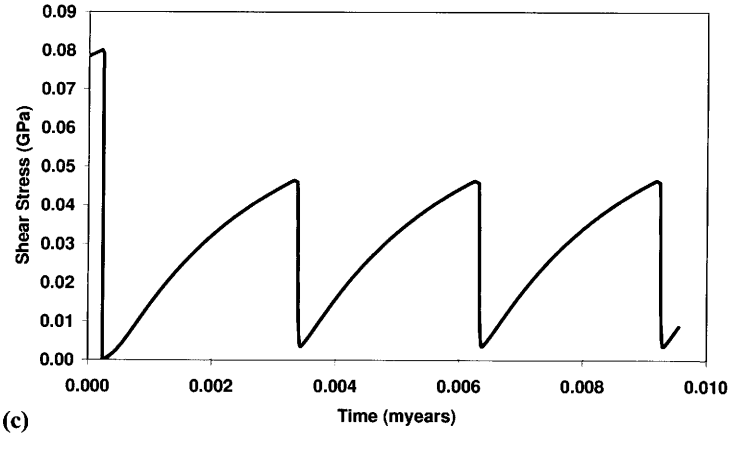

(c)

Fig. 18. History of **(a)** rock competency, **(b)** failure function and **(c)** shear stress. After a short transient period, the system finds its limit cycle.

tribution of fracture network statistics across a field is a necessary input to reservoir simulators used to optimize production.

The dynamics of the fracture network in our model is based on a statistical representation. For example, consider a set of fractures of length L with normal $\underline{n}$ for a 3D spectrum of normal orientations. Then the rate of change for L in the rock-fixed frame takes the form:

$$\frac{dL}{dt} = R(L, a, p, \Theta, \underline{\underline{\sigma}}) \tag{16}$$

where the fracture extension rate R depends on the normal stress σ, the wetting phase fluid pressure p and the texture Θ of the surrounding rock, and c is the aperture of the n-fracture. A similar equation for the fracture aperture is developed (see Tuncay *et al.* (2000*b*) for further details).

Let η' be the number density of sites at which fractures may nucleate. By definition of the undeformed rock $\eta' = \eta$ (being the original, depositional value of η') but η' can differ from due to changes in rock texture from diagenesis or mechanical processes. In the simplest case where fracture nucleation sites are not created or destroyed, η' obeys the conservation equation $\partial\eta'/\partial t + \nabla \cdot (\eta' u) = 0$. In a macrovolume element of volume V there are $V\eta'$ fractures and hence a fracture void space $V\eta' \pi L^2 a$ where a and L are the aperture and length (radius) of the assumed penny-shaped fractures, respectively. To compute the dilatation, we focus on a fixed volume V_m of solids and follow its change in a time δt. The volume of the unfractured rock V_{unfr} is related to V_m and the porosity ϕ_m of the unfractured rock via $V_{unfr} = V_m + \phi_m V_{unfr}$. Hence, $V_{unfr} = V_m / (1 - \phi_m)$. The total volume V of the sample of rock containing V_m is then:

$$V = (1 - \phi_m)^{-1} V_m + V\Delta \tag{17}$$

where $\Delta = \eta' \pi L^2 a$. With this, the volume of rock $V(t)$ at time t for fixed volume of solids V_m (considered incompressible and not to expand thermally or react) is given by:

$$V(t) = V_m (1 - \phi_m)^{-1} (1 - \Delta) \tag{18}$$

Noting that

$$tr\dot{\underline{\underline{\varepsilon}}}^{fr} = \lim_{\delta t \to 0} \frac{V(t + \delta t) - V(t)}{V(t)\, \delta t} \tag{19}$$

one obtains

$$tr\dot{\underline{\underline{\varepsilon}}}^{fr} = [1 - \Delta]^{-1} \frac{D\Delta}{Dt} \tag{20}$$

The tensor character of the fracture-mediated deformation is related to the directions of each fracture through its normal to the fracture plane. Consider the expression:

$$\dot{\varepsilon}_{kl}^{fr} = [1 - \Delta]^{-1} \frac{D}{Dt} (\Delta n_k n_l) \tag{21}$$

Here D/Dt represents a material time derivative; however, now, it also must account for the rotation of the fracture normals as they change direction with flexure, shearing or other deformation. Note that the trace of this expression agrees with the earlier result for the dilatation. Finally, this expression agrees with simple cases wherein all fractures are parallel.

In our model, a finite (but representative) number of fracture orientations is accounted for. We use the fracture kinetics formulation of Ortoleva 1994*a*, and Sonnenthal & Ortoleva (1994). However, here we replace the least compressive stress in the formulation by the stress component normal to each fracture plane. This allows calculation of fracture length and aperture for each fracture orientation. For example, if we assume that only vertical fractures can occur as for a one-dimensional problem, since the stress component normal to any vertical plane is the same because of the symmetry, an isotropic fracture network develops. In three-dimensional problems, our proposed algorithm has the power to predict a complex fracture network with preferential orientations dictated by the structure of the stress tensor.

Since the fracture network is well defined, the anisotropic fracture permeability can be calculated approximately. The anisotropic fracture permeability of a fracture network consisting of a single fracture orientation is given by:

$$K_{ij}^{fr} = \lambda(\delta_{ij} - n_i n_j) \tag{22}$$

where $\underline{n}$ is the unit normal to the fracture plane and $\underline{\underline{K}}^{fr}$ is the fracture permeability. The parameter λ can be approximated by:

$$\lambda = \beta \phi_{fr} \frac{a^2}{12} \tag{23}$$

Here β is a factor accounting for the connectivity of fractures. For large fracture lengths and dense networks β approaches unity whereas for small

fracture lengths and low fracture densities it vanishes (Oda 1986). Oda (1985, 1986) proposed that this coefficient should be a function of a dimensionless second-order tensor of fracture geometry. He called this tensor the fabric tensor (Oda 1982). In this study β is taken as unity. In our computation, the total fracture permeability is taken to be the sum of fracture permeabilities for all orientations. It is assumed that fluid flow is slow and the disturbance at fracture intersections is negligible. Summation of fracture permeability of different sets is inadequate when the fracture density is lower than the percolation threshold (Berkowitz 1995; Odling 1992; Bour & Davy 1998). Another limitation is due to the surface roughness of fractures. In this study fracture aperture is assumed to be constant in a particular fracture. The spatial distribution of fracture aperture alters the fracture permeability. Waite *et al.* (1998) measured water flow through a sinusoidal fracture to compare sinusoidal flow with parallel-plate flow. Their experimental and numerical results showed that a sinusoidal fracture has a significantly lower permeability and for the sinusoidal geometry the effective aperture is very close to the minimum value of the normal aperture. Thomson & Brown (1991) showed that the directional non-uniformities in the fracture surface are more important than the degree of surface roughness.

Conclusions

The examples presented above illustrate the complex set of factors that yield the disposition of the present-day fracture system. The latter is the product of a history of these factors and thereby often has little correlation with one or a few other present-day factors. The extensive set of rock and fluid parameters at each point within the crust makes inversion of seismic data difficult except for the simplest cases. Therefore the integration of standard seismic techniques with comprehensive modelling presented here should provide a new oppurtunity for predicting the location and characterization of fractured zones in the subsurface. We believe that our Basin RTM simulator is uniquely suited for this purpose.

This project was supported by the Office of Science of the US Department of Energy (grant no. DE-FG02–91ER14175) and the Gas Research Institute (contract no. 5097–260–3779).

References

ABRIOLA, L. M. & RATHFELDER, K. 1993. Mass-balance errors in modeling 2–phase immiscible flows – causes and remedies. *Advances in Water Resources*, **16**, 223–239.

BERKOWITZ, B. 1995. Analysis of fracture network connectivity using percolation theory. *Mathematical Geology*, **27**, 467–483.

BERRYMAN, J. G. 1980. Long-wavelength propagation in composite elastic media I. Spherical inclusions, *Journal of the Acoustics Society of America*, **68**, 1809–1819.

BERRYMAN, J. G. 1986, Effective medium approximation for elastic constants of porous solids with microscopic heterogeneity. *Journal of Applied Physics*, **59**, 1136–1140.

BOUR, O. & DAVY, P. 1998. On the connectivity of three-dimensional fault networks. *Water Resources Research*, **34**, 2611–2622.

BYERLEE, J. D. 1990. Friction, overpressure and fault normal compression. *Geophysical Research Letters*, **17**, 2109–2112.

DESAI, C. S. & SIRIWARDANE, H. J. 1984. *Constitutive laws for engineering material.* Prentice-Hall, New Jersey.

DEWERS, T, & ORTOLEVA, P. 1994. Nonlinear dynamical aspects of deep basin hydrology: Fluid compartment formation and episodic fluid release. *American Journal of Science*, **294**, 713–755.

DRÜKER-PRAGER, D. C. & PRAGER, W. 1952. Soil mechanics and plastic analysis or limit design. *Quarterly of Applied Mathematics*. **10**, 157–165.

HUYAKORN, P. S., PANDAY, S. & WU, Y. S. 1994. A three-dimensional multiphase flow for assessing NAPL contamination in porous and fractured media, 1. Formulation. *Journal of Contaminant Hydrology*, **16**, 109–130.

LARSON, K. W., WAPLES, D. W. FU, H. & KODAMA, K. 1993. Predicting tectonic fractures and fluid flow through fractures in basin modeling. *In:* DORE, A. G. (ed.) *Basin Modeling: Advances and Applications*.Norwegian Petroleum Society. Special Publications, **3**, Elsevier, Amsterdam, 373–383.

LUO, X. & G. VASSEUR. 1996. Geopressuring mechanism of organic matter cracking: numerical modeling. *AAPG Bulletin*, **80**, 856–873.

LUO, X., VASSEUR, G., POUYA, A., LAMOUREUX-VAR, AND, V. & POLIAKOV, A. 1998. Elastoplastic deformation of porous medium applied to the modeling of compaction at basin scale. *Marine and Petroleum Geology*, **15**, 145–162.

MAUBEUGE, F. & LERCHE, I. 1993. A north Indonesian basin: geo, thermal and hydrocarbon generation histories. *Marine and Petroleum Geology*, **10**, 231–245.

MAUBEUGE, F. & LERCHE, I. 1994. Geopressure evolution and hydrocarbon generation in a north Indonesian basin: two-dimensional quantitative modeling. *Marine and Petroleum Geology*, **104**, 104–115.

ODA, M. 1982. Fabric tensor for discontinous geological materials. *Soils and Foundations*, **22**, 96–108.

ODA, M. 1985. Permeability tensor for discontinous rock masses. *Geotechnique*, **35**, 483–495.

ODA, M. 1986. An equivalent continuum model for coupled stress and fluid flow analysis in jointed rock masses. *Water Resources Research*, **22**, 1845–1856.

ODLING, N.E. 1992. Network properties of a two-dimensional natural fracture pattern. *Pure and Applied Geophysics*, 138, 95–114.

ORTOLEVA, P. (ed.) 1990. Self-organization in geological systems. *Earth-Science Reviews*, **29**(1–4),

ORTOLEVA, P. 1992. *Nonlinear Chemical Waves*. John Wiley and Sons: New York.

ORTOLEVA, P. 1994*a*. *Geochemical Self-Organization*. Oxford University Press, Oxford.

ORTOLEVA, P. 1994*b*. Basin compartmentation: definitions and mechanisms. *In:* ORTOLEVA, P. (ed.) *Basin Compartments and Seals*. AAPG Memoir **61**, 39–51.

ORTOLEVA, P. 1998. *Basin compartment fundamentals*. GRI Topical Report (Contract No. GRI-97/0097). Gas Research Institute:Chicago.

ORTOLEVA, P., MAXWELL, J. M., PAYNE, D., SIBO, W. & COMER, J. 1997. Naturally fractured reservoirs and compartments: a pedictive basin modeling approach. *In:* HOAK, T. E., KLAWITTER, A. L. & BLOMQUIST, P. K. (eds) *Fractured Reservoirs: Characterization and Modeling*, Rock Mountain Association of Geologist Guidebooks, 67–102, Denver, RMAG.

OZKAN G, & ORTOLEVA, P. 2000. Evolution of the gouge particle size distribution: A Markov model. *Pure and Applied Geophysics*, **157**(3), 449–468.

OZKAN, G., TUNCAY, K. & ORTOLEVA, P. 1998. Process-based fault seal/conduit prediction. In: *AAPG Annual Convention Abstracts, Salt Lake City, UT, May 17–28, 1998* (CD-ROM format).

PAYNE, D. F., TUNCAY, K., PARK, A., COMER, J. & ORTOLEVA, P. 2000. A reaction-transport-mechanical approach to modelling the interrelationships between gas generation, overpressuring, and fracturing –Implications for the Upper Cretaceous natural gas reservoirs of the Piceance Basin, Colorado. *AAPG Bulletin*, **84**, 545–565.

RICE, J.R. 1975. Continuum mechanics and thermodynaimcs of plasticity in relation to microscale deformation mechanisms. *In:* ARGON, A. S. (ed.), *Constitutive Equations in Plasticity*. MIT Press: Cambridge, MA.

RICE, J. R. 1992. Fault stress states, pore pressure distributions, and the weakness of the San Andreas Fault. *In:* EVANS, B. & WONG, T.-F. (eds) *Fault Mechanics and Transport Properties in Rocks*. Academic Press, London, 475–503.

ROBERTS, S. J. & NUNN, J. A. 1995. Episodic fluid expulsion from geopressured sediments. *Marine and Petroleum Geology*, **12**, 195–204.

SAKRANI, K. 1996. *A unified texture and mineralogy dependent model for rock deformation*. PhD dissertation, Indiana University, Bloomington.

SCHNEIDER, F., POTDEVIN, J. L., WOLF, S. & FAILLE, I. 1996. Mechanical and chemical compaction model for sedimentary basin simulators. *Tectonophysics*, **263**, 307–317.

SLEEP, N. H. & BLANPIED, M. L. 1994. Ductile creep and compaction: a mechanism for transiently increasing fluid pressure in mosly sealed fault zones. *Pure and Applied Geophysics*, **143**, 9–40.

SONNENTHAL, E. & ORTOLEVA, P. 1994. Numerical simulations of overpressured compartments in sedimenatary basins. *In:* ORTOLEVA, P. (ed.) *Basin compartments and seals*. AAPG Memoir **61**, 403–416.

THOMSON, M. E. & BROWN, S. R. 1991. The effect of anisotropic surface roughness on flow and transport in fractures. *Journal of Geophysical Research*, *96*, 21923–21932.

TUNCAY, K. & ORTOLEVA, P. 2000. Salt tectonics as a self-organizing process: a three dimensional reaction, transport and mechanics model. *Journal of Geophysical Research*, **106**, 803–818.

TUNCAY, K., PARK, A. & ORTOLEVA, P. 2000*a*. A forward model of three dimensional fracture orientation and characteristics. *Journal of Geophysical Research*, **105**, 16719–16735.

TUNCAY, K., PARK, A. & ORTOLEVA, P 2000*b*. Sedimentary basin deformation: An incremental stress rheology approach. *Tectonophysics*, **323**, 77–104.

TUNCAY, K., KHALIL, A. & ORTOLEVA, P. 2001. Failure, memory and cyclic fault movement. *Bulletin of Seismological Society of America*, **91**, 538–552.

UNGERER, P., BURRUS, J., DOLIGEZ, B., CHENET, P. Y. & BESSIS, F. 1990. Basin evaluation by integrated two-dimensional modeling of heat transfer, fluid flow, hydrocarbon generation, and migration. *AAPG Bulletin*, **74**, 309–335.

WAITE, M.E., GE, S., SPETZLER, H. & BAHR, D. B. 1998. The effect of surface geometry on fracture permeability: A case study using a sinusoidal fracture. *Geophysical Research Letters*, **25**, 813–816.

WANG, C. & XIE, X. 1998. Hydrofracturing and episodic fluid flow in shale-rich basins –A numerical study. *AAPG Bulletin*, **82**, 1857–1869.

ZIENKIEWICZ, O. C. & CORMEAU, I. C. 1974. Visco-plasticity–plasticity and creep in elastic solids—A unified numerical solution approach. International *Journal for Numerical Methods for Engineering*, **8**, 821–845.